

The Luminosity Function of QSO Host Galaxies

Timothy S. Hamilton,^{1,2,3} Stefano Casertano,^{1,3,4} and David A. Turnshek^{2,3}

ABSTRACT

We present some results from our *HST* imaging study of 71 QSO host galaxies. The objects are selected to have $z \leq 0.46$ and total absolute magnitude $M_V \leq -23$. The aim of this initial study is to investigate the composition of the sample with respect to host morphology and radio loudness, as well as derive the QSO host galaxy luminosity function. We have analyzed 49 objects with *WFPC2* images using procedures we developed and combined our results with similarly-derived results from the literature for the remaining 22 objects. The host galaxies span a narrow range of luminosities and are exceptionally bright, much more so than normal galaxies, usually greater than a few times L_V^* . The QSO hosts are almost equally divided between three subclasses: radio-loud QSOs with elliptical hosts, radio-quiet QSOs with elliptical hosts, and radio-quiet QSOs with spiral hosts. Radio-loud QSOs with spiral hosts are extremely rare. The hosts of two QSOs went undetected; one is radio loud and the other is a radio quiet BAL QSO. The elliptical host luminosity distribution of the radio-loud QSOs differs significantly from both the elliptical and spiral host luminosity distributions of the radio-quiet QSOs, which generally are compatible. The same is true when considering the unresolved nuclear luminosity of these subclasses. Elliptical hosts are typically twice as luminous as spiral hosts, and the hosts of radio-loud QSOs are typically 2.5 times as luminous as those of radio-quiet QSOs. We consider and discuss possible selection effects. Using a weighting procedure, we derive the combined luminosity function of QSO host galaxies. Subject to systematic uncertainties in normalization procedures, we find that the luminosity function of low-redshift QSO hosts closely corresponds to the bright tail of the normal local galaxy luminosity function. The probability of a galaxy of luminosity L_V hosting a QSO is $P \approx (L_V/7.2L_V^*)^3$, approaching $P \approx 1$ for $L_V > 7.2L_V^*$, where L_V^*

¹Space Telescope Science Institute, 3700 San Martin Drive, Baltimore, MD 21218, USA

²Department of Physics & Astronomy, University of Pittsburgh, Pittsburgh, PA 15260, USA

³email: hamilton@ra.phyast.pitt.edu, stefano@stsci.edu, turnshek@quasar.phyast.pitt.edu

⁴on assignment from the Space Sciences Division of the European Space Agency

corresponds to $M_V^* = -22.35$ ($H_0 = 50$ km/s/Mpc, $q_0 = 0.5$) and a QSO is defined to be an object with total nuclear plus host light $M_V \leq -23$.

1. Introduction

Much has been learned about the properties of QSO host galaxies since they were first imaged almost three decades ago (Kristian 1973). Early results include establishing a positive correlation between host and nuclear QSO luminosities (Hutchings, Crampton, & Campbell 1984) and indications of a morphological difference between radio-loud and radio-quiet QSOs, with the former more likely to be in elliptical hosts and the latter in spiral hosts (Malkan, Margon, & Chanan 1984). Working in the near-infrared, where the luminosity contrast is more favorable to the host galaxy, Dunlop et al. (1993) show that QSO hosts are typically drawn from the bright end of the galaxy luminosity function (in agreement with Hutchings et al.). McLeod & Rieke (1994a,b), also using near-infrared data, find that hosts of radio-quiet QSOs are typically represented by an exponential (spiral disk) light profile (in agreement with Malkan et al.), and that high-luminosity QSOs generally have brighter hosts than low-luminosity QSOs (in agreement with Hutchings et al.).

High-resolution space-based images taken with the *Hubble Space Telescope* (*HST*) make the imaging of the host galaxy much easier. The first, and to date one of the largest, systematic *HST* studies of QSO hosts is by Bahcall, Kirhakos, & Saxe (1997), who study 20 of the most luminous nearby QSOs. They can discern the morphology of the hosts, and they discover that, while radio-loud QSOs are found only in ellipticals or interacting systems, radio-quiet QSOs can be in ellipticals, spirals or interacting systems. They also find that QSO hosts do not follow a Schechter (1976) luminosity function and are instead found at systematically high luminosities. More recent studies strengthen and expand on these results. McLure et al. (1999) confirm that QSO hosts are generally luminous, and also determine that, even for radio-quiet QSOs, the hosts are often ellipticals or bulge-dominated. Furthermore, elliptical hosts appear to follow the same luminosity-surface brightness relation as field elliptical galaxies (Hamabe & Kormendy 1987).

In this contribution we focus on the luminosity distribution of a large sample of QSO hosts observed with the *Wide Field and Planetary Camera 2* (*WFPC2*) aboard *HST* (§2). We have collected and reanalyzed archival images of 49 QSOs with $M_V \leq -23$ mag (total nuclear + host light) and redshifts $0.06 \leq z \leq 0.46$. We have taken an inclusive approach in our sample selection, imposing no additional selection criteria on the QSOs besides those of total absolute magnitude and redshift, while some of the previous work on QSO hosts has focused on specific classes of QSOs: radio loud (Lehnert et al. 1999), intrinsically very

bright (Bahcall et al. 1997), and so on. For each we have subtracted the nuclear light component using two-dimensional image fits and have derived the luminosity and size of the underlying host galaxy by fitting both an $r^{1/4}$ and an exponential light profile (§3). In addition, we use published results on 22 other QSO hosts (§4) which were analyzed in the same way and satisfy the same selection criteria as our sample of 49 QSOs. Given the total number of objects considered, more than triple that of previous studies, we can effectively sample the general QSO population for redshifts $z \leq 0.46$, and derive a global luminosity function for their host galaxies (§5) which is not grossly affected by selection criteria. This luminosity function is compared with that of normal galaxies, and selection effects/biases and other issues are discussed (§6). Conclusions are then summarized (§7).

We confirm previous results that host galaxies of QSOs are significantly more luminous than typical luminous L_V^* galaxies. We also consider the relationship between host morphology and QSO radio loudness. Elliptical hosts are, on average, about 0.7 mag brighter than spiral hosts, and hosts of radio-loud QSOs are, on average, about a magnitude brighter than hosts of radio-quiet QSOs. Subject to systematic uncertainties in normalization procedures, we find that the combined low-redshift QSO host luminosity function closely resembles an extension of the bright end of the local galaxy luminosity function. In approximate terms, the probability of a galaxy of luminosity L_V hosting a QSO (with total $M_V \leq -23$) is $P \approx (L_V/7.2L_V^*)^3$, approaching $P \approx 1$ for $L_V > 7.2L_V^*$, where L_V^* corresponds to $M_V^* = -22.35$.

Throughout this Letter, we adopt a Friedman cosmology with $H_0 = 50$ km/s/Mpc and $q_0 = 0.5$. We have converted the results of other researchers to this cosmology when comparing our results to theirs.

2. Sample Selection

Our sample includes 71 QSOs with total magnitudes $M_V \leq -23$ and redshifts $0.06 \leq z \leq 0.46$ with available *WFPC2* observations in F606W or redder filters. The objects are listed in Table 1. For 49 QSOs, we have analyzed or reanalyzed *HST* archival imaging observations in a systematic and uniform manner, and the results are reported in §3. For the remaining 22 QSOs, we have relied on published analysis, as reported in §4.

The absolute magnitude selection ($M_V \leq -23$) aims at including only historically conventional QSOs. However, since the selection is based on the *combined* magnitude of the host and nucleus, lower-luminosity nuclei, down to $M_V \approx -19$, are in fact included in our sample. We have not excluded these objects from our analysis, since they would be present

in most magnitude-selected ground-based samples.

We limit our analysis to objects with $z \leq 0.46$, in order to ensure that *HST* resolution permits a reliable separation between the host and nuclear component. At $z \approx 0.4$, a typical host with a half-light radius of 9 kpc has an apparent radius of $1''.4$, which corresponds to 14 pixels in the *Wide Field Camera (WFC)* or 31 pixels in the *Planetary Camera (PC)*. The light from the host should therefore be clearly separated from that of the nucleus. In fact, the host galaxy could not be convincingly detected in only two of the 71 QSOs in our sample; these two are listed as such in Table 1.

3. Measurement Technique

Even at *HST* resolution, the light of the unresolved nuclear central source significantly affects the extended light distribution of the host galaxy. A careful subtraction of the central point source is needed in order to measure the properties of the host accurately. The following is a brief description of our technique, which is largely similar to that of Remy et al. (1997).

Because of the complex structure of the *HST WFPC2* Point Spread Function (PSF), our analysis procedure has three principal steps: (1) A model of the PSF is fitted to the central point source, in order to determine its subpixel position and the telescope focus, which affects the shape of the PSF. (2) The luminosity of the PSF is determined by fitting the PSF plus a simple galaxy model to the light in the central region of the image; this accounts for the small gradient in the galaxy light that would remain uncorrected if the PSF were fitted in isolation. (3) The fitted PSF is subtracted, and the properties of the host are determined from fitting the residual light.

The fitting of a model PSF, as opposed to an observed PSF, is dictated by both opportunity and quality considerations. Since we rely on archival data, in most cases we do not have a PSF observation taken at the same time as the QSO image. The PSF in *WFPC2* varies with time as a consequence of short and long term changes in the telescope focus. Thus, using a PSF observed at other times does not generally yield a good subtraction of the nuclear light. Also, the undersampled nature of *WFPC2* images make PSF subtraction very difficult, unless both PSF and image have been properly dithered. Under most circumstances, a cleaner PSF subtraction can be achieved by using a model PSF produced by the so-called TinyTim software (Krist & Burrows 1995), provided both focus and subpixel positions are explicitly fitted (Remy et al. 1997; Surdej et al. 1997). This also results in photometry which is comparable in accuracy to using an observed PSF.

3.1. First step: fitting the PSF

The model PSF is constructed from a set of artificial PSFs, created using the TinyTim software (Krist & Hook 1999). TinyTim uses a detailed model of the telescope and camera optics, including the zonal errors in the primary and secondary mirrors, to produce a good wavelength-dependent approximation of the resulting PSF. However, the PSF structure changes significantly depending on both the telescope focus and on exactly how the point source is centered with respect to the pixel grid. The telescope focus changes with time due to “breathing,” which is the thermal expansion and contraction of the spacecraft due to changes in its attitude relative to the Sun. Breathing typically changes the relative positions of the primary and secondary mirrors by about $5\mu\text{m}$.

Therefore, we produce PSF models oversampled 11 times, i.e., on virtual pixels 11 times smaller than actual detector pixels, and for focus positions that range from $-10\mu\text{m}$ to $+10\mu\text{m}$ in $1\mu\text{m}$ steps. Each PSF is then aligned with various offsets with respect to the true pixel grid and resampled to the actual detector resolution, including the estimated pixel spread function described in the TinyTim documentation. The best fit to the light distribution in the central few pixels identifies the subpixel position and the estimated focus of the observation. If the PSF is not saturated, we can achieve a precision of ≈ 0.01 pixels in the central position and $\approx 1\mu\text{m}$ in the focus position. During this procedure, the light of the extended galaxy, which varies little over the scale of the PSF, is treated as a constant background.

In some cases, several of the pixels at the core are overexposed and saturated on the CCD. These pixels provide no information and are masked from all fits. The pixels immediately adjacent to them are also masked, because the CCD “blooming” effect could have altered the pixels’ intensity values. Our technique works also in the presence of saturation, although the focus position is determined less accurately. Most images have either no saturation or a small amount which does not completely cover the PSF core.

Once the position and focus have been found, a PSF of angular size large enough to cover the host image is created using these parameters and is used for subsequent analysis.

3.2. Second step: distinguishing the QSO and host galaxy light

A second two-dimensional fit distinguishes the light of the QSO from that of the resolved host galaxy, simultaneously fitting both parts. In this step, the model PSF’s brightness is scaled to match the QSO nuclear brightness, while a galaxy model is fitted to the host. The host model accounts for ellipticity, position angle, brightness, size, and

a simple morphological classification based on radial profile. We consider two surface brightness models, each of which is convolved with the PSF: the de Vaucouleurs $r^{1/4}$ law, $I(\tilde{r}) = I(0) \exp[-7.67(\tilde{r}/\tilde{r}_{1/2})^{1/4}]$, which is typical of elliptical galaxies, and the exponential law, $I(\tilde{r}) = I(0) \exp[-\tilde{r}/\tilde{r}_e]$, typical of spirals. Here, \tilde{r} is the elliptical radius, $\tilde{r} = (x^2 + \alpha^2 y^2)^{1/2}$, where x and y are aligned with the major and minor axes of the ellipse, respectively, and $\alpha = a/b$, where a is the semi-major axis and b is the semi-minor axis. The half-light radius $\tilde{r}_{1/2}$ is the elliptical radius enclosing half the total light as projected onto the sky; for the exponential model, $\tilde{r}_{1/2} = 1.68\tilde{r}_e$.

In seven cases, namely 3C 215, PG 0052+251, MRK 1014, PG 1402+261, Q 1222+1010, PG 1001+291 and PKS 0736+01, the automated fitting procedure did not produce a good match to the central point source, most often because of complex host features at very small radii. For these cases, we manually subtracted an increasingly luminous central point source until the residuals were smooth. Consequently, the resulting nuclear and host magnitudes for these objects are somewhat subjective and more uncertain.

For most objects, the host morphology was assigned simply on the basis of the best-fitting (lowest χ^2) model: elliptical if the $r^{1/4}$ model fitted best, spiral if the exponential model did. We overruled the automatic classification in six cases. Four hosts, those of PHL 909, PKS 0312–77, PG 1358+04 and PKS 1004+13, yield a spiral classification after the automated fit, but their radial profile was judged to follow an $r^{1/4}$ law more closely overall and they show no obvious evidence of spiral arms; they are reclassified as ellipticals, and the $r^{1/4}$ model is used in our subsequent analysis. Two hosts, those of MRK 1014 and PG 1309+355, have their radial profile outside their central bulges well represented by the $r^{1/4}$ law, yet show clear evidence of spiral arms. They are thus classified as spiral, although the best-fitting $r^{1/4}$ law is used in the analysis. Note that we have been able to identify late-type spiral structure in hosts at redshift as high as $z = 0.4$. Except for these six cases, we have kept the morphological assignments determined by the best-fitting models.

For spiral hosts with a visible bulge, we use masks to fit the bulge and disk separately. The bulge is fitted first, and its model is subtracted from the entire image before the disk is fitted. Bars, if present, are masked out of the fit altogether, though they are used in determining the host’s total magnitude. Based on visual inspection, some hosts appear to have undergone recent, strong interactions which have severely distorted their appearances from those of a normal elliptical or spiral, and we have noted these in Table 1. However, in this contribution we will not report on the details of the interaction in the hosts.

3.3. Third step: extracting the magnitudes

Using the fitted parameters, we then subtract the properly scaled PSF from the QSO image, leaving the host galaxy. We measure the light in this subtracted image, within an aperture large enough to encompass the visible extent of the host. Outside the aperture, we extrapolate the host model to a radius of infinity and add this contribution to the light contained within the aperture, yielding the apparent magnitude of the host galaxy. The measurements are not based on the models alone because the host profiles often deviate from strict $r^{1/4}$ or exponential laws, creating noticeable differences between magnitudes derived from the model alone and magnitudes obtained in the way described above. For certain objects we have found that such differences exist when comparing our observed (measured) host magnitudes to those calculated by the researchers using fitted model parameters (see §3.4 and §4).

The observations were made in *WFPC2* F606W or redder filters and the observed apparent magnitudes have been transformed to rest frame V , converted to absolute magnitude in our adopted cosmology ($H_0 = 50$ km/s/Mpc, $q_0 = 0.5$), and reported in Table 1. Normal k -corrections are accounted for in this process.

3.4. Comparison with other methods

There are other analysis techniques which have been used in studies with criteria similar to our own. The method of Bahcall et al. (1997) is different from ours. They are able to use stellar PSFs taken at the time of the observations, while we generally cannot. They observed a set of four stars for the PSFs, chosen to have colors similar to QSOs. The PSF is subtracted by scaling it until the χ^2 between it and the QSO image is minimized. The best-fitting of the four PSF stars is used in each case. Elliptical and spiral host models are then fit to the residual in an annular region $r > 1''0$, avoiding the core of the QSO. Bahcall et al. try one- and two-dimensional models, and adopt the two-dimensional results in the end.

McLure et al. (1999) also use stellar observations for the PSFs in their analysis, employing two-point dithering to improve the sampling (and therefore the subpixel centering), with the PSF stars being chosen to closely match the typical $B-V$ colors of QSOs. Their host fitting technique is similar to ours, with the host and QSO being fitted simultaneously. They used a two-dimensional host model, assuming either a strict $r^{1/4}$ or exponential law profile, and varying the host model's size, luminosity, ellipticity and position angle, as well as the nuclear luminosity. Separately, they try the technique of using

a model with the radial profile having a variable exponent, β . A true exponential law would have $\beta = 1.00$, and a de Vaucouleur law would appear as $\beta = 0.25$. They achieve similar classifications using this technique, but their adopted M_{host} values are based on the former method.

4. Literature data

Of the 71 QSOs in our sample, we have independently analyzed 49 QSOs so far. The results for the remaining 22 QSOs have been taken from various sources in the literature. The majority of these, 16, come from the study by Bahcall et al. (1997), while the others come from a number of different works (see references noted in Table 1).

In order to verify the consistency between our results and those of others, we have considered 23 cases in which we have reanalyzed an image which has published results. We note in particular that Bahcall et al. (1997) provide the results of both their one-dimensional and two-dimensional model fits; while they adopt the two-dimensional magnitudes in their analysis, we find that their one-dimensional magnitudes agree better with ours, and thus adopt their one-dimensional magnitudes in our analysis. For the 4 images in common, the one-dimensional data of Bahcall et al. (1997) are dimmer than ours by 0.2 ± 0.3 , and the two-dimensional data are dimmer by 0.6 ± 0.3 . We find that our *host* magnitudes are brighter than all literature results, on average, by 0.56 ± 0.37 mag. The difference depends systematically on the technique used; the method of McLure et al. (1999) is the most similar to ours, and indeed, our magnitudes are only slightly brighter than theirs, by 0.09 ± 0.08 mag for 4 objects. The differences between our results and other results reported in the literature are further discussed in §6.3, as are the possible effects on the shape of the host luminosity function which we derive.

5. The Luminosity Function of QSO Host Galaxies

5.1. Subclasses and the unweighted absolute magnitude distribution of QSO hosts

With 69 detected QSO hosts in our sample, we are able to quantitatively investigate the properties of the host galaxy luminosity function, and also to begin considering issues related to host morphology and radio loudness.

As noted in §2, the hosts of two QSOs were not convincingly detected; one is a

radio-loud QSO (MRC 0022–197) and the other is a radio-quiet QSO (PG 0043+039) with Broad Absorption Lines (BALs) in its spectrum (Turnshek et al. 1994). For one spiral (MS 2159.5–5713) we have no radio information. Consequently, the two QSOs with undetected hosts are excluded from our analysis; MS 2159.5–5713 is excluded from analyses requiring radio information.

It is of interest to consider whether the remaining elliptical and spiral hosts in our sample are drawn from different parent populations. This might also be related to possible selection effects and biases (§6.2). We can consider these objects in terms of a binary classification yielding four subclasses. The nuclear and host magnitudes for these objects separated by subclass are plotted in Figure 1. Our sample is divided almost evenly into three subclasses: radio-loud QSOs with elliptical hosts (designated “LE”, 23 objects), radio-quiet QSO with elliptical hosts (designated “QE”, 23 objects), and radio-quiet QSOs with spiral hosts (designated “QS”, 19 objects). Membership in the fourth subclass, radio-loud QSOs with spiral hosts (designated “LS”, 3 objects), is rare. First we discuss the rare LS subclass.

Two of the three radio-loud spirals, 3C 277.1 and MC 1548+114A, are at redshifts $z > 0.3$ and have little detail visible, but both appear to have large tidal arms which may be responsible for the exponential profile being the better model. However, it is possible that they are simply interacting cases and not normal spirals. The third, PG 1309+355, appears to be a *bona-fide* spiral which is radio-loud according to the data and definition of Kellermann et al. (1989), having a radio-to-optical flux density ratio of ≈ 18 , in excess of the ratio of 10 which they use to define a radio-loud object. With the exception of PG 1309+355, we thus confirm the result of Bahcall et al. (1997) that radio-loud QSOs are almost exclusively found in elliptical or interacting hosts, while radio-quiet QSOs may be found in elliptical, spiral or interacting systems. The host absolute magnitudes of the radio-loud spirals were found to lie in the range $-22.9 > M_V > -24.0$, consistent with our overall host absolute magnitude distribution.

To check whether the host and nuclear luminosities in each of the three major subclasses are consistent with being drawn from similar parent populations, we have applied two-sample Kolmogorov-Smirnov (K-S) tests to each combination of subclasses. The detailed results are listed in Table 2. Comparison of the LE and QE subclasses shows that their host luminosity distributions differ at a significance of 99.8%, while their nuclear luminosity distributions differ at a significance of 90.4%. Comparison of the LE and QS subclasses shows that both their host and nuclear luminosity distributions differ at a significance $> 99.9\%$. However, the host and nuclear luminosity distributions of the QE and QS subclasses are reasonably compatible. In summary, the host and nuclear luminosity

distributions of the LE subclass is significantly more sharply peaked and brighter than the QE subclass and especially more sharply peaked and brighter than the QS subclass (see Figure 1).

We have also compared the host and nuclear luminosities of all ellipticals (“E”, 46 objects) to all spirals (“S”, 23 objects), and the host and nuclear luminosities of all radio-loud QSOs (“L”, 26 objects) to all radio-quiet QSOs (“Q”, 42 objects). The results are also shown in Table 2 and indicate that all of these distributions are different at a significance $\geq 99.3\%$.

In Figure 2 we present the number distribution of QSO hosts as a function of their absolute magnitude. This distribution is almost entirely contained within a range of 2.5 mag, from $M_V \approx -22$ to -24.5 , with a median of $M_V \approx -23.4$. It is reasonably well-fitted by a Gaussian with a peak at $M_V = -23.44$ and a 1σ width of 0.94 mag. There is an indication of a small tail at faint magnitudes, but the numbers are too small for any quantitative conclusions. Note that, since all but two hosts are clearly detected, the lack of faint hosts is *not* due to difficulties in detecting them.

The individual distributions for the subclasses are *qualitatively similar* to the combined, with a well-defined broad peak and a very small faint tail, but each distribution is offset and somewhat narrower than the combined. When considering host morphology in detail, it becomes apparent that elliptical hosts are typically brighter than spiral hosts, indeed about twice (≈ 0.7 mag) as luminous. The median absolute magnitude is $M_V \approx -23.6$ for ellipticals and $M_V \approx -22.9$ for spirals. The differences between the hosts of radio-loud and radio-quiet QSOs are also noticeable. Radio-loud QSO hosts are typically 2.5 times (≈ 1.0 mag) more luminous than radio-quiet QSOs hosts. The median absolute magnitude is $M_V \approx -23.9$ for radio-loud QSO hosts and $M_V \approx -22.9$ for radio-quiet QSO hosts.

5.2. The weighted number distribution of QSO host absolute magnitudes

The 71 QSOs in our sample comprise $\approx 7\%$ of all known QSOs within the magnitude range of our sample in the catalog of Véron-Cetty & Véron (1998; hereafter VCV). However, since our selection of QSOs to include in this study is based on the availability of *HST* observations, they may not adequately represent the characteristics of all low-redshift QSOs. In particular, our sample may be systematically biased as a function of apparent luminosity and redshift: nearer and brighter objects are more accessible, and therefore more likely to be selected for study. We therefore apply a simple weighting technique to approximately correct for any redshift- and magnitude-dependent selection effects.

Our procedure for weighting the distribution function to derive a corrected or unbiased distribution function is based on a replacement method as follows. For each of the 982 QSOs in VCV within our selected magnitude and redshift range, we pick a representative object in our observed sample with approximately the same total (nuclear + host) magnitude M_{tot} and redshift z . The representative object is chosen randomly with a Gaussian probability distribution that depends on the difference in absolute magnitude and redshift. We choose a Gaussian width of 0.5 mag in absolute magnitude and 0.07 in redshift. These widths are chosen to ensure that most catalog objects have several sample objects within about 1σ in both magnitude and redshift; if the widths are too narrow, regions of the (M_{tot}, z) plane that contain few sample objects would yield a luminosity function that depends too heavily on those few objects.

Each object, i , in our observed sample is then assigned a weight, w_i , which is simply the number of times it is selected by the random process. The resulting weighted distribution function is shown as the unshaded histogram in Figure 3. The error bars reflect the nominal counting error defined as $\sigma_{bin} = (\sum_i(w_i^2))^{1/2}$, where the sum is over all objects in the bin. Note that this error is an upper limit for the Poisson uncertainty in the distribution function in that bin, in that it assumes that the host magnitude is not correlated with redshift or total magnitude; any correlation makes the assignment process less random and therefore reduces the counting uncertainty.

The weighted distribution function has a more pronounced faint tail than the unweighted function, the result of counting faint objects, which are underrepresented in the observed sample, multiple times. However, the median of the distribution is essentially the same as for the unweighted distribution, $M_V \approx -23.4$. The best-fitting Gaussian has its peak at $M_V = -23.64$ and a 1σ width of 0.60 mag, but this is not a particularly good fit at the faint end. We have also attempted to fit a Schechter (1976) function to the distribution, finding parameters $M_V^* = -23.15$ and $\alpha = 0.65$, but this yields a poor fit to the peak and the bright end.

Since the morphologies of VCV hosts are generally unknown, we cannot weight the elliptical and spiral distributions separately as we did in §5.1. However, since we are dealing with relatively nearby QSOs, we can perform a weighting for radio loudness if we take the objects in VCV with 6 cm flux densities greater than 0.1 Jy to be radio-loud and those with lower values or no detections to be radio-quiet. Using this definition for radio loudness, we have derived a weighted distribution function of QSO hosts, separated in terms of hosts of radio-loud QSOs (“L”, 26 objects) and hosts of radio-quiet QSOs (“Q”, 42 objects). These individual weighted distributions (shaded) are also shown in Figure 3. The radio-loud and radio-quiet distributions are essentially unchanged between the weighted and unweighted

versions.

5.3. The luminosity function of QSO host galaxies

We have used the QSO luminosity function of Boyle et al. (2000) to derive a normalization for our weighted host distribution function, turning it into a QSO host galaxy luminosity function. Boyle et al. (2000) have analyzed a ground-based sample of over 6000 QSOs to derive a QSO luminosity function for the total (nuclear + host) light. They parameterize the luminosity function in terms of a two-power-law function, $\Phi(M_B, z) = \Phi^*/(10^{-0.4(\alpha+1)[M_B-M_B^*(z)]} + 10^{-0.4(\beta+1)[M_B-M_B^*(z)]})$ and use a polynomial function for the evolution of $M_B^*(z)$ in redshift, $M_B^*(z) = M_B^*(0) - 2.5(k_1z + k_2z^2)$, where $\alpha = 3.60$, $\beta = 1.77$, $M_B^*(0) = -22.39$, $k_1 = 1.31$, $k_2 = -0.25$ and $\Phi^* = 6.8 \times 10^{-7}$ objects $\text{Mpc}^{-3} \text{mag}^{-1}$. The data of Boyle et al. (2000) is limited to redshifts of $z \geq 0.35$, and at the low-redshift end it does not span a large range in total absolute magnitude. Thus, we have restricted our consideration to redshifts of $0.35 \leq z \leq 0.46$, where our sample overlaps with theirs, and to total absolute magnitudes of $-23.00 \geq M_V(\text{total}) \geq -24.61$, extending no more than one magnitude brighter than $M_B^*(0.405)$. We use $z = 0.405$ for the function, since it is the average of the range we consider. Since the total absolute magnitudes of the QSOs in the survey of Boyle et al. (2000) are likely dominated by nuclear luminosity, we assume $B - V \approx 0.0$.

Integrating the two-power-law function over the range $-23.0 \geq M_V(\text{total}) \geq -24.61$, with $z = 0.405$, we find 7.5×10^{-7} QSOs Mpc^{-3} . Over the same total absolute magnitude interval, with $0.35 \leq z \leq 0.46$, there are 228 objects in the VCV catalog. Dividing the integrated function by 228, we obtain a normalization factor of $3.3 \times 10^{-9} \text{Mpc}^{-3}$. Multiplying our weighted host distribution by this normalization factor (and by a factor of 2 to account for our 0.5 magnitude bin width and by a factor of 2/3 for our 1.5 mag bin for the faintest bin) converts our distribution into a QSO host luminosity function in units of QSO hosts $\text{Mpc}^{-3} \text{mag}^{-1}$. This QSO host luminosity function is shown in Figure 4. We note that in Figure 4 we also show how removing objects with nuclear luminosities fainter than $M_V = -23$ affects the derived luminosity function.

6. Discussion

Here we elaborate on some of the results of this work. A more thorough discussion will be made when we consider the other properties of the sample in detail.

6.1. Comparison of the QSO host and normal galaxy luminosity functions

To compare our QSO host galaxy luminosity function (§5.3) with that of normal galaxies, we use the normal galaxy luminosity function of Metcalfe et al. (1998). The Schechter (1976) luminosity function parameters which describe their V-band luminosity function in our cosmology are $\alpha = -1.2$, $M_V^* = -22.35$, and $\Phi^* = 8.5 \times 10^{-2}$ galaxies Mpc^{-3} . The most relevant uncertainty in their normal galaxy luminosity function is at the bright end, where it is less well-constrained due to the dearth of luminous galaxies in surveys. The least luminous QSO host used in our analysis is relatively luminous, with $M_V \approx -20.1$, and the median of our QSO host luminosity function is at $M_V \approx -23.4$, about a magnitude brighter than the M_V^* “knee” of the normal galaxy luminosity function. The normal galaxy luminosity function is also shown in Figure 4.

The most luminous part of the normal galaxy luminosity function is seen to fall slightly below the QSO host luminosity function, but owing to the uncertainty due to poor number statistics for luminous galaxies, the two distributions are clearly compatible. Thus, we conclude that the luminosity function of QSO hosts essentially corresponds to the bright tail of the normal galaxy luminosity function. We can therefore use these results to estimate the fraction of galaxies at a given absolute magnitude which host a QSO. The QSO host luminosity function divided by the normal galaxy luminosity function results in a determination of the fraction of galaxies hosting QSOs as a function of luminosity. The determination of this fraction, from division of the results shown in Figure 4, is shown in Figure 5. This result is essentially the probability of a galaxy of luminosity L_V hosting a QSO, where a QSO is defined to be an object with total nuclear plus host light $M_V \leq -23$. In approximate terms, this probability can be expressed simply as $P \approx (L_V/7.2L_V^*)^3$, approaching $P \approx 1$ for $L_V > 7.2L_V^*$, where L_V^* corresponds to $M_V^* = -22.35$ ($H_0 = 50$ km/s/Mpc, $q_0 = 0.5$). This relation is also shown in Figure 5. We note that the accuracy of these results are subject to the inherent systematic uncertainties in normalization procedures for both the local galaxy luminosity function and our low-redshift QSO host galaxy luminosity function.

This conclusion, that the luminosity function of QSO hosts corresponds to the bright tail of the normal galaxy luminosity function, is similar to the conclusion reached by Smith et al. (1986) in their ground-based study of AGN/QSO hosts. The current data are of course better than what was available to them, so we believe that the conclusion is now considerably stronger. Moreover, Smith et al. (1986) also derived the probability of a galaxy hosting a QSO as a function of host luminosity. Our parameterization of $P(L_V)$ is different than theirs, but again the idea is conceptually the same. We find the discussion presented by Smith et al. (1986) to still be relevant.

6.2. Radio-loud and radio-quiet QSOs with elliptical hosts

We showed in §5.1 that the QE subclass has dimmer, broader, and more asymmetrical host and nuclear luminosity distributions than the LE subclass. However, there is some overlap in the QE and LE distributions. Within this overlap region there do not appear to be gross differences in host luminosity, yet there must be some property which affects the amount or nature of the fuel available to the central engine for radio emission. The possible causes of this effect should be investigated more closely by using the members of these two subclasses of elliptical hosts to examine other properties of these QSOs, including environmental clues.

6.3. Selection effects and biases

A bright QSO may be expected to hide a dim host, and the more distant it is, the harder the host will be to detect. However, we are able to see hosts that are 3 – 4 magnitudes dimmer than their nuclear QSO light, and we find that this holds true for host sizes ranging from smaller than $\approx 0''.5$ to $\approx 4''.0$, beyond which there is little relevant data. Considering the faint end of the host distribution in particular, the commonly accepted division between QSOs and less luminous AGN is $M_V \leq -23$ (for $H_0 = 50$ km/s/Mpc), and our data suggest that we could see a host as dim as $M_V \approx -19$ to -20 for a QSO of this magnitude. In general, considering that the host magnitudes span a noticeably smaller range than the nuclear QSO magnitudes (Figure 1), combined with the fact that we have failed to detect a host in only two cases so far, makes us confident that our host luminosity function is not strongly biased by missing very dim hosts.

The ellipticals outnumber the spirals in our sample, making up $\approx 70\%$ of the total. However, due to *HST* target selection effects, this may not be representative of all QSOs in this redshift range. For example, we have confirmed, with only one clear exception, that radio-loud QSOs are found in elliptical or interacting hosts (§5.1), while radio-quiet QSOs may be found in either ellipticals, spirals or interacting cases. The fraction of radio-loud QSOs in our sample is $\approx 37\%$. Among optically-selected samples in this redshift range, the fraction of radio loud QSOs is more likely $\approx 10\%$ (Hooper et al. 1996), although other studies put it as high as $\approx 20\%$ (Kellermann et al. 1989; Hooper et al. 1995). In either case, we have a significantly higher fraction of radio-loud QSOs than the actual population, and this may indicate that we have a higher fraction of elliptical hosts as well. Nevertheless, the weighting procedure we used in §5.2 should account for these effects.

As previously mentioned, the apparent host magnitudes derived from our analysis are

generally brighter than those found in the corresponding literature data, by an average of 0.56 ± 0.37 mag, which is about the width of our luminosity bins. We believe that at least part of difference lies in our direct measurement of the apparent host magnitude from the PSF-subtracted image, without relying on a simple galaxy model, except at large radii. In theory, if the host model fit is weighted inversely to the square of the Poisson noise in the image, use of the model will result in slightly fainter magnitudes in comparison to use of the actual host image. In practice, comparing our host apparent magnitudes with the results we would get from the models alone, we find differences of ≈ 0.25 mag when using $1/\sigma$ weighting. We have checked one example by refitting with flat weighting. This cuts the magnitude difference in half, but the $1/\sigma$ weighting scheme is the appropriate way to handle noise. We have tried to minimize the problem by relying more on the image than on the model. In any case, the differences between the results in the literature and our own appear to depend in part on the particular analysis method used. If we adjust the results in the literature according to these differences, we find the effect on the total host luminosity function to be relatively minor. The unweighted absolute magnitude distribution becomes more symmetric, but the value of the median remains nearly unchanged. The effect on the weighted luminosity function is insignificant.

6.4. Comparisons with some other studies

There have been a few other large-sample studies of QSO hosts with selection criteria similar to our own. Of the space-based *HST* ones, the two largest, those of Bahcall et al. (1997) and of McLure et al. (1999), have been included in our luminosity function.

The sample of Bahcall et al. (1997) includes 20 QSOs with redshifts $z < 0.3$ and $M_V < -24.4$, making them the most luminous objects in the nearby universe. The distribution of their host magnitudes is similar to that of our whole sample. They find that, on average, the hosts of radio-loud QSOs are one magnitude brighter than the hosts of radio-quiet QSOs, a result matched in our whole sample. They also report the hint of a luminosity difference between elliptical and spiral hosts, but caution that it may be artificial, a consequence of fitting the host model to the outer ($r \geq 1''.0$) region of the host and the different profiles of the spiral and elliptical models inside that radius. Our analysis has shown that this luminosity difference is real, with the ellipticals being ≈ 0.7 mag brighter than spirals. Bahcall et al. (1997) also note that their data are inconsistent with host magnitudes being distributed according to the Schechter (1976) function, a conclusion also consistent with our findings.

The sample of McLure et al. (1999) includes 15 QSOs with a redshift range of

$0.1 \leq z \leq 0.35$. Assuming $V - R \approx 1.0$, the hosts of McLure et al. (1999) are at the dimmer end of our distribution, peaking in the $-22.5 > M_V > -23.0$ bin and extending no brighter than $M_V = -23.5$, just above our median value. They find that radio-quiet QSOs with hosts brighter than $M_R = -24$ ($M_V \approx -23$) are in elliptical hosts, however we find that one-third of our radio-quiet QSO hosts brighter than this are spirals.

7. Conclusions

1. We have assembled a sample of 71 *HST* *WFPC2* imaging observations of luminous QSOs (total nuclear plus host light $M_V \leq -23$ in our adopted cosmology with $H_0 = 50$ km/s/Mpc and $q_0 = 0.5$) in the redshift interval $0.06 \leq z \leq 0.46$. We have derived results on QSO host and nuclear luminosities and host morphology, and compile results on radio loudness. Of the 71 QSOs, 49 were analyzed by us using procedures developed for this work, while in the remaining 22 cases the results could be reliably taken from the literature.

2. The host galaxies span a narrow range of luminosities and are exceptionally bright, much more so than normal galaxies, usually greater than a few times L_V^* .

3. The hosts are almost equally divided between subclasses of radio-loud QSOs with elliptical hosts (23 objects), radio-quiet QSOs with elliptical hosts (23 objects), and radio-quiet QSOs with spiral hosts (19 objects). Radio-loud QSOs with spiral hosts (at most 3 objects) are extremely rare. The hosts of two QSOs went undetected; one is radio loud and the other is a radio quiet BAL QSO.

4. The elliptical host luminosity distribution of the radio-loud QSOs differs significantly from both the elliptical and spiral host luminosity distributions of the radio-quiet QSOs. However, the latter two distributions are generally compatible. Elliptical hosts are typically twice as luminous (≈ 0.7 mag) as spiral hosts, and the hosts of radio-loud QSOs are typically 2.5 times as luminous (≈ 1 mag) as those of radio-quiet QSOs.

5. Using a weighting procedure, we derive the combined luminosity function of low-redshift QSO host galaxies. Subject to systematic uncertainties in normalization procedures, the luminosity function of QSO hosts closely corresponds to the bright tail of the local galaxy luminosity function, where a QSO is defined in historically conventional terms, i.e., total nuclear plus host light has $M_V \leq -23$. For this definition, the probability of a galaxy of luminosity L_V hosting a QSO is $P \approx (L_V/7.2L_V^*)^3$, approaching $P \approx 1$ for $L_V > 7.2L_V^*$, where L_V^* corresponds to $M_V^* = -22.35$.

Further investigations of the properties of this sample should be useful.

This research was supported by a grant from the Space Telescope Science Institute. Use was made of the NASA Extragalactic Database (NED). We would like to thank Dr. Sandhya Rao for discussions about luminosity functions and comments on the manuscript.

REFERENCES

- Bahcall, J. N., Kirhakos, S., & Saxe, D. H. 1997, *ApJ*, 479, 642
- Boyce, P., et al. 1998, *MNRAS*, 298, 121
- Boyce, P., et al. 1996, *ApJ*, 473, 760
- Boyce, P., Disney, M., & Bleaken, D. 1999, *MNRAS*, 302, L39
- Boyle, B. J., Shanks, T., Croom, S. M, Smith, R. J., Miller, L., Loaring, N., & Heymans, C. 2000, *MNRAS*, 317, 1014
- Dunlop, J. S., Taylor, G. L., Hughes, D. H., & Robson, E. I. 1993, *MNRAS*, 264, 455
- Hamabe, M., & Kormendy, J. 1987, in *Structure and Dynamics of Elliptical Galaxies*, ed. T. de Zeeuw (Dordrecht, Holland: IAU), 379
- Hooper, E. J., Impey, C. D., Foltz, C. B., & Hewett, P. C. 1995, *ApJ*, 445, 62
- Hooper, E. J., Impey, C. D., Foltz, C. B., & Hewett, P. C. 1996, *ApJ*, 473, 746
- Hutchings, J. B., Crampton, D., & Campbell, B. 1984, *ApJ*, 280, 41
- Kellermann, K. I., Sramek, R., Schmidt, M., Shaffer, D. B., & Green, R. 1989, *AJ*, 98, 1195
- Krist, J., & Burrows, C. J., 1995, *Applied Optics*, 34, 4951
- Krist, J., & Hook, R., 1999, *The Tiny Tim User's Guide*, (Baltimore: STScI), available at <http://www.stsci.edu/software/tinytim/tinytim.pdf>
- Kristian, J. 1973, *ApJ*, 179, L61
- Lehnert, M., van Breugel, W., Heckman, T., & Miley, G. 1999, *ApJS*, 124, 11
- Malkan, M. A., Margon, B., & Chanan, G. A. 1984, *ApJ*, 280, 66
- Metcalf, N., Ratcliffe, A., Shanks, T., & Fong, R. 1998, *MNRAS*, 294, 147
- McLeod, K. K., & Rieke, G. H. 1994a, *ApJ*, 420, 58
- McLeod, K. K., & Rieke, G. H. 1994b, *ApJ*, 431, 137
- McLure, R. J., Kukula, M. J., Dunlop, J. S., Baum, S. A., O'Dea, C. P., & Hughes, D. H. 1999, *MNRAS*, 308, 377

- Remy, M., Surdej, J., Baggett, S., & Wiggs, M. 1997, in *1997 HST Calibration Workshop*, ed. S. Casertano et al. (Baltimore: STScI), 374
- Schechter, P. 1976, *ApJ*, 203, 297
- Smith, E. P., Heckman, T. M., Bothun, G. D., Romanishin, W., & Balick, B. 1986, *ApJ*, 306, 64
- Surdej, J., Baggett, S., Remy, M., & Wiggs, M. 1997, in *1997 HST Calibration Workshop*, ed. S. Casertano et al. (Baltimore: STScI), 386
- Turnshek, D. A., et al. 1994, *ApJ*, 428, 93
- Véron-Cetty, M. P., & Véron, P. 1998, *A Catalog of Quasars and Active Galactic Nuclei* (ESO Sci. Rept. No. 18) (8th ed.; Garching: ESO)

Morphological and Radio-loudness Divisions

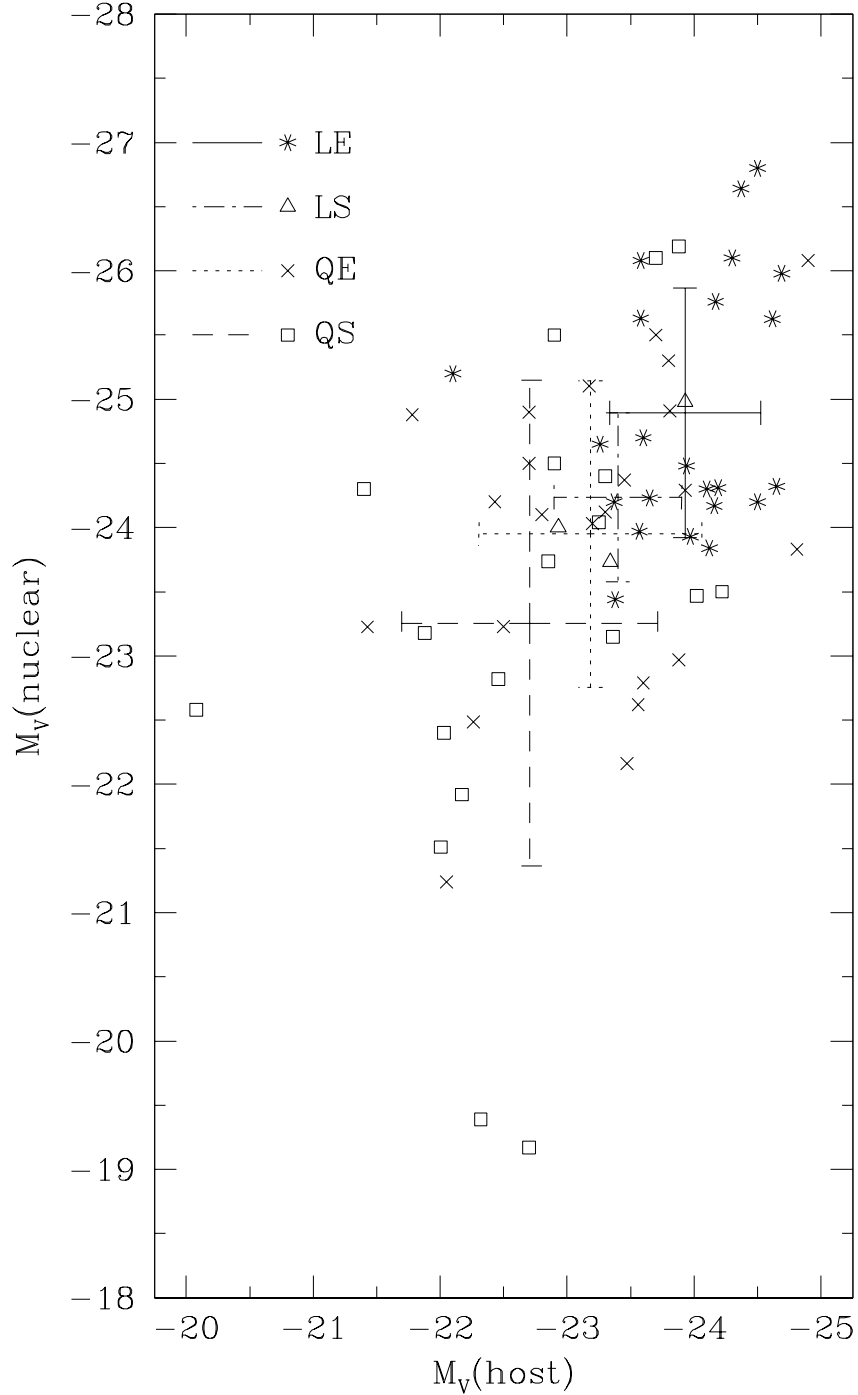


Fig. 1.— Distribution of morphological and radio properties of the sample with respect to host and nuclear luminosities. Individual * symbols are radio-loud QSOs in ellipticals (LE), × symbols are radio-quiet QSOs in ellipticals (QE), square symbols are radio-quiet QSOs in spirals (QS), and triangular symbols are radio-loud QSOs in spirals (LS). The RMS error bars for each subclass are overlaid, centered on the mean of each distribution according to

Unweighted Distribution Function of QSO Hosts

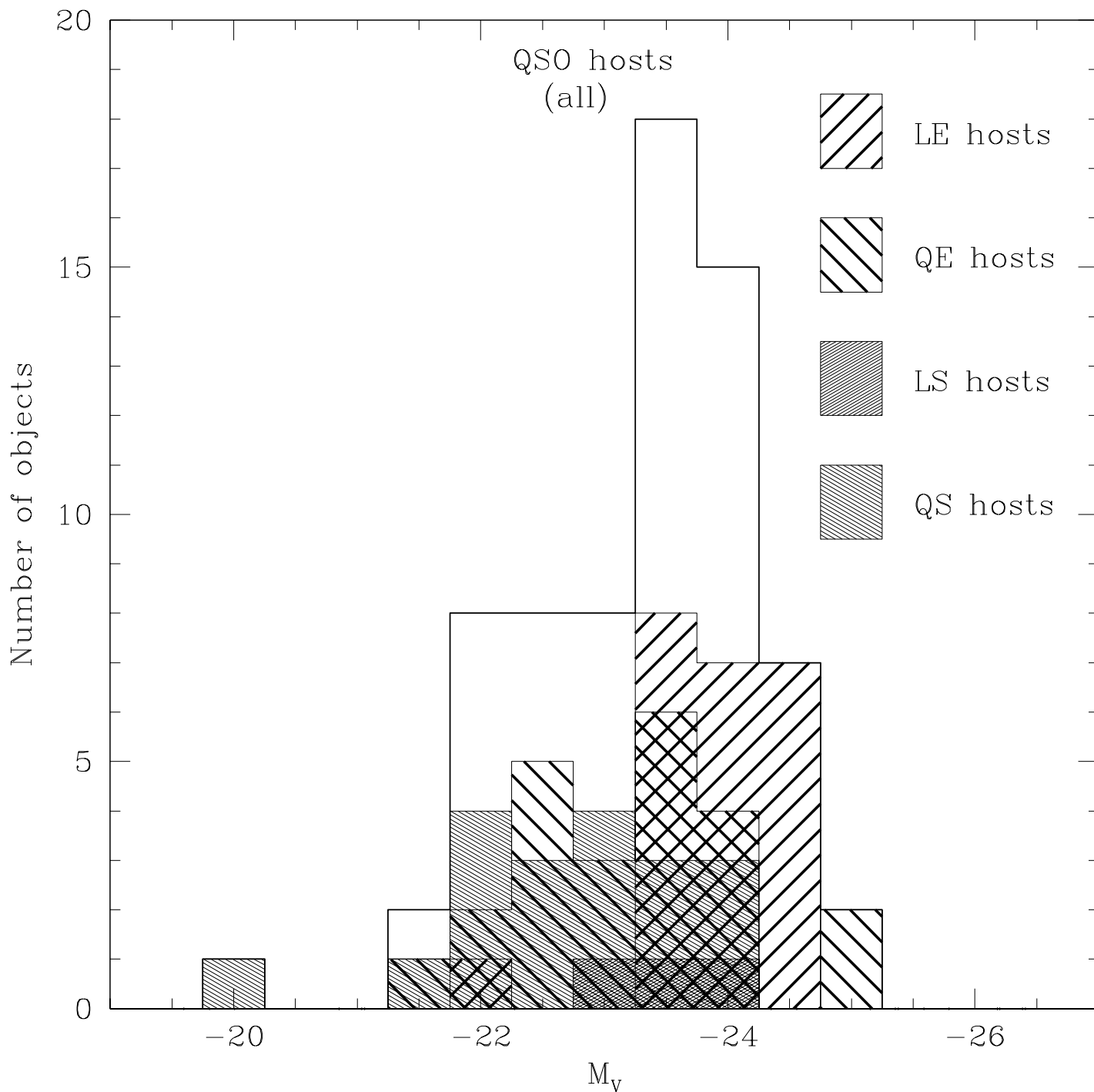


Fig. 2.— The unweighted absolute magnitude distribution function of all QSO hosts (unshaded histogram). The four interior shaded histograms show the individual host distributions of radio-loud QSOs in ellipticals (LE), radio-quiet QSOs in ellipticals (QE), radio-loud QSOs in spirals (LS), and radio-quiet QSOs in spirals (QS).

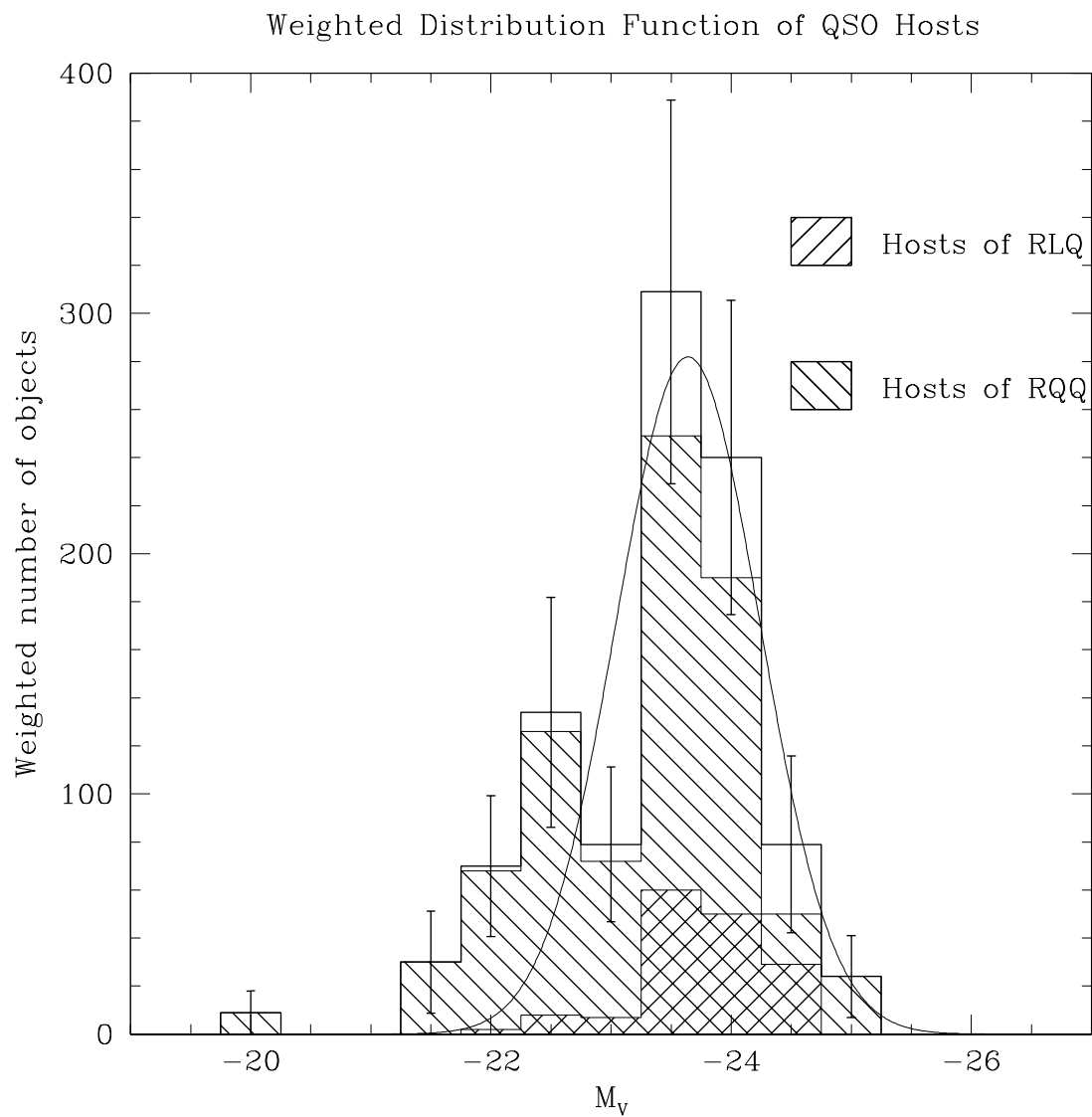


Fig. 3.— The combined weighted absolute magnitude distribution function of QSO hosts (unshaded histogram) fitted with a Gaussian. The two interior shaded histograms show the distribution of host absolute magnitudes for radio-loud QSOs and radio-quiet QSOs.

Comparison of QSO Host and Normal Galaxy Luminosity Functions

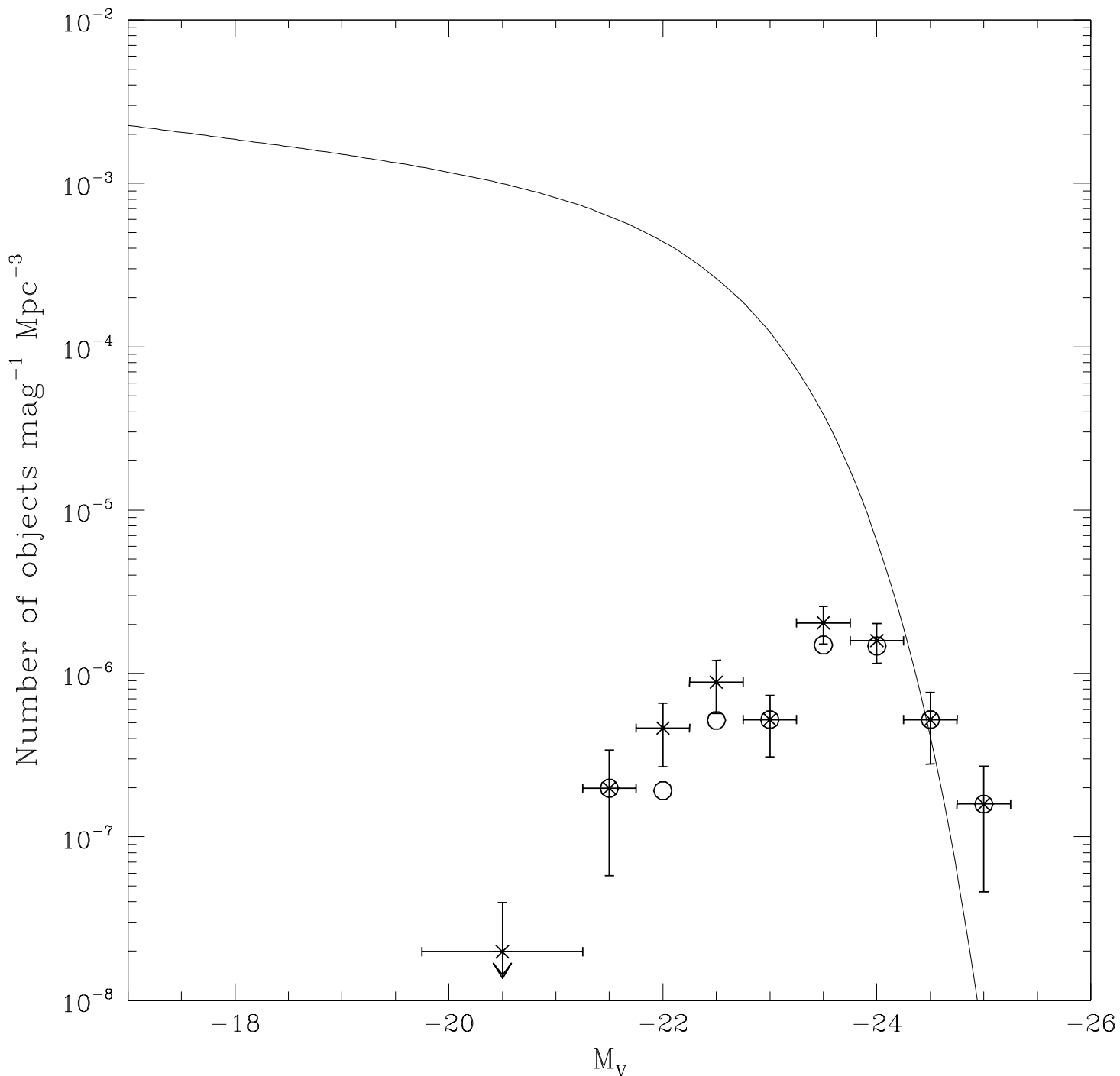


Fig. 4.— The combined luminosity function of QSO host galaxies for our sample compared to the normal galaxy luminosity function of Metcalfe et al. (1998). Crosses show the derived luminosity function for the entire sample, while open circles show the derived luminosity function for QSOs with nuclear magnitudes brighter than $M_V = -23$. The low-redshift QSO host galaxy luminosity function is seen to closely correspond to the bright end of the normal

Fraction of Galaxies Hosting QSOs

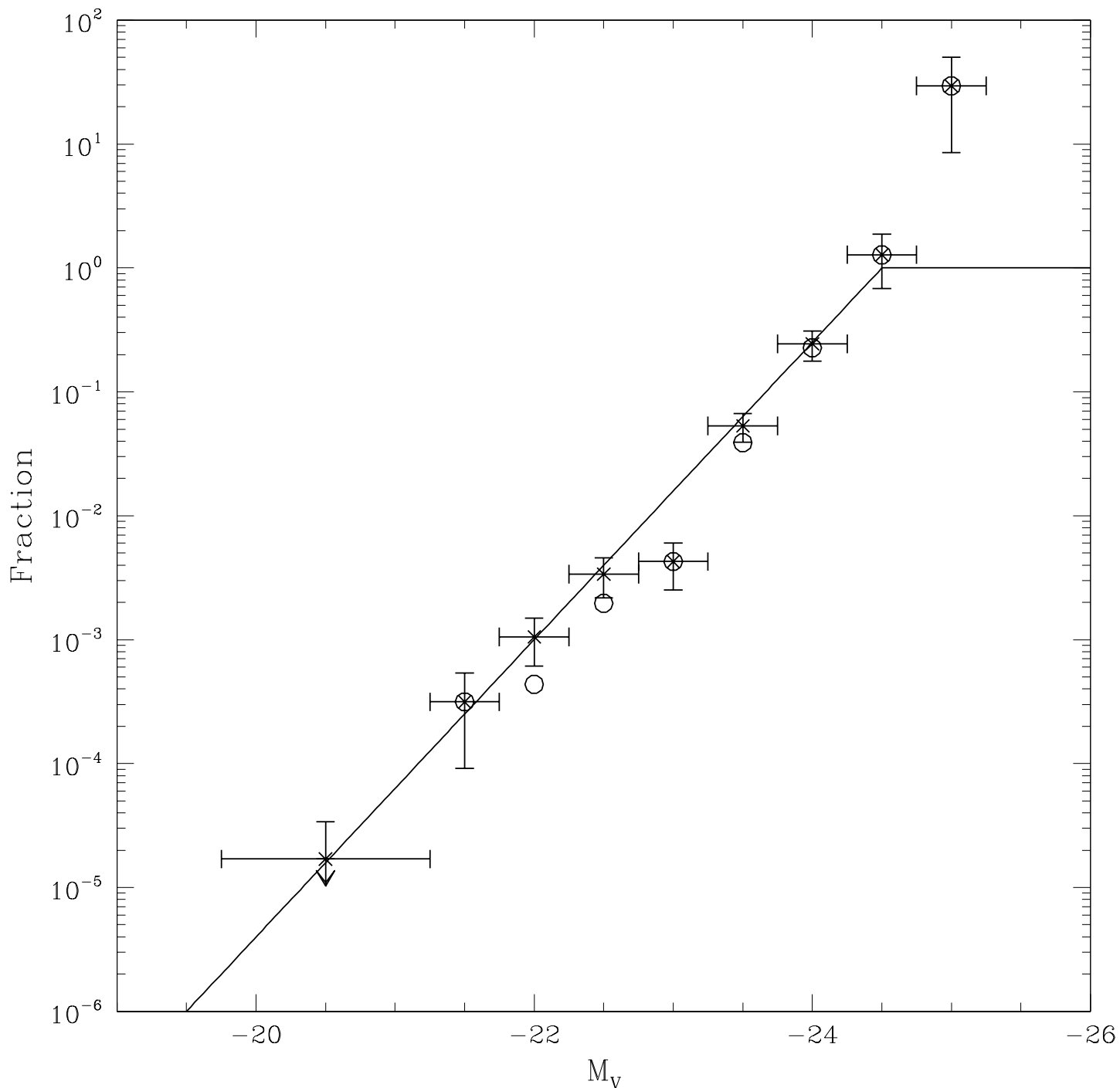


Fig. 5.— The low-redshift QSO host galaxy luminosity function divided by the normal local galaxy luminosity function, yielding the probability that a galaxy of absolute magnitude M_V will host a QSO. Crosses show this result for the entire sample, while open circles show this result for QSOs with nuclear magnitudes brighter than $M_V = -23$. The fit shown in the figure is specified in the text.

Table 1. Observations

RA (J2000)	Dec (J2000)	Name	$M_{V,nuc}$ ¹	$M_{V,host}$ ¹	Morph ²	RL/RQ	Reference ³
00 23 11.1	+00 35 16.5	Q 002311+003517	−22.79	−23.60	E	Q	TW
00 24 03.7	−02 45 27.8	Q 002403−024500	−22.97	−23.88	E	Q	TW
00 24 32.5	−29 28 55.5	MRC 0022−297	L	TW
00 45 46.6	+04 11 15.8	PG 0043+039	Q	TW
00 54 55.7	+25 25 47.2	PG 0052+251	−24.04	−23.25	S	Q	TW
00 57 11.6	+14 45 24.5	PHL 909	−24.37	−23.45	E	Q	TW
01 03 13.0	+02 21 10.5	UM 301	−24.12	−23.30	E	Q	TW
01 36 22.4	+20 57 14.7	3C 47	−24.17	−24.16	E	L	TW
01 37 39.0	+33 09 22.0	3C 48	−26.08	−23.58	EI	L	B99
01 39 59.0	+01 31 01.6	PHL 1093	−23.93	−23.97	E	L	TW
01 59 52.2	+00 23 50.1	MRK 1014	−23.50	−24.22	S	Q	TW
02 02 05.1	−76 20 04.3	PKS 0202−76	−25.63	−23.58	E	L	TW
02 07 49.5	+02 43 43.0	NAB 0205+02	−24.3	−21.4	S	Q	B97
02 47 42.2	+19 40 09.4	Q 0244+194	−23.23	−22.50	E	Q	TW
03 00 31.6	+02 40 06.7	US 3498	−19.39	−22.32	S	Q	M99
03 11 46.7	−76 51 40.8	PKS 0312−77	−24.48	−23.94	E	L	TW
03 18 07.9	−34 25 52.2	0316−346	−26.1	−23.7	IS	Q	B97
03 43 30.0	+04 57 48.6	3C 93	−23.44	−23.38	E	L	TW
04 52 32.4	−29 53 41.0	IR 0450−2958	−23.18	−21.88	SI	Q	B96
07 39 18.0	+01 37 04.6	PKS 0736+01	−23.97	−23.57	E	L	TW
07 57 57.8	+39 20 34.7	MS 07546+3928	−24.03	−23.20	E	Q	TW
08 04 35.3	+64 59 53.9	IR 0759+6508	−22.58	−20.08	SI	Q	B96
08 04 55.0	+21 20 45.7	MS 0801.9+2129	−22.82	−22.46	S	Q	TW
08 39 52.6	−12 14 42.7	3C 206	−24.20	−23.37	E	L	TW
09 06 31.9	+16 46 11.5	3C 215	−24.31	−24.19	E	L	TW
09 25 57.7	+19 53 45.4	PG 0923+201	−25.10	−23.17	E	Q	TW
09 46 50.7	+13 19 52.6	MS 0944.1+1333	−24.20	−22.43	E	Q	TW
09 56 48.7	+41 15 47.2	PG 0953+414	−25.5	−22.9	S	Q	B97
10 04 00.4	+28 55 20.2	PG 1001+291	−26.19	−23.88	S	Q	TW
10 07 29.1	+12 48 33.3	PKS 1004+13	−25.63	−24.62	E	L	TW
10 14 56.2	+00 34 21.2	PG 1012+008	−24.4	−23.3	SI	Q	B97
10 31 52.5	−14 16 10.9	HE 1029−1401	−24.9	−22.7	E	Q	B97
11 02 38.2	+72 46 09.9	MS 1059.0+7302	−21.52	−22.00	S	Q	TW
11 19 06.7	+21 18 39.3	PG 1116+215	−25.3	−23.8	E	Q	B97
12 04 42.2	+27 54 12.0	PG 1202+281	−24.1	−22.8	E	Q	B97
12 12 27.9	+12 42 54.5	Q 121228+124254	−22.62	−23.56	E	Q	TW
12 19 23.1	+06 38 26.8	PG 1216+069	−24.88	−21.78	E	Q	B98
12 20 37.2	+17 18 24.4	1218+1734	−23.84	−24.12	E	L	TW
12 21 45.9	+75 19 06.5	MS 1219.6+7535	−22.49	−22.26	ES	Q	TW
12 25 10.7	+09 54 38.8	Q 1222+1010	−23.47	−24.02	S	Q	TW
12 25 15.0	+12 18 40.2	Q 1222+1235	−24.32	−24.65	E	L	TW
12 29 09.9	+02 03 02.3	3C 273	−26.8	−24.5	E	L	B97
12 32 03.6	+20 09 29.2	PG 1229+204	−22.40	−22.03	S	Q	TW
12 42 39.5	+17 38 22.6	LBQS 1240+1754	−24.29	−23.93	E	Q	TW
12 46 30.2	+16 45 23.5	LBQS 1243+1701	−23.83	−24.81	E	Q	TW
12 52 25.2	+56 34 36.4	3C 277.1	−23.73	−23.34	S	L	TW
13 05 36.1	−10 33 36.2	PG 1302−102	−26.1	−24.3	E	L	B97
13 09 47.0	+08 19 49.5	PG 1307+085	−24.5	−22.7	E	Q	B97
13 12 16.3	+35 14 36.7	PG 1309+355	−24.98	−23.93	S	L	TW

Table 1—Continued

RA (J2000)	Dec (J2000)	Name	$M_{V,nuc}$ ¹	$M_{V,host}$ ¹	Morph ²	RL/RQ	Reference ³
14 00 33.9	+04 04 46.8	PG 1358+04	−26.08	−24.90	E	Q	TW
14 04 38.7	+43 27 07.5	1403+434	−24.91	−23.81	EI	Q	HM95
14 05 12.9	+25 55 17.7	PG 1402+261	−24.50	−22.90	S	Q	TW
14 19 05.7	−13 10 56.5	MS 1416.3−1257	−23.23	−21.43	E	Q	TW
14 27 33.6	+26 32 52.9	B2 1425+267	−25.76	−24.17	E	L	TW
14 29 08.6	+01 17 13.0	MS 1426.5+0130	−23.74	−22.85	S	Q	TW
14 46 49.1	+40 34 34.7	PG 1444+407	−25.5	−23.7	E	Q	B97
15 14 39.2	+36 50 37.7	B2 1512+37	−26.64	−24.37	E	L	TW
15 22 30.7	−06 44 43.1	MS 1519.8−0633	−21.92	−22.17	S	Q	TW
15 47 47.5	+20 51 33.1	3C 323.1	−24.3	−24.1	E	L	B97
15 50 42.5	+11 19 54.2	MC 1548+114A	−24.00	−22.93	SI	L	TW
16 37 46.5	+11 49 49.7	MC 1635+119	−21.24	−22.05	E	Q	M99
17 04 38.3	+60 44 51.4	3C 351	−25.2	−22.1	E	L	B98
21 37 48.1	−14 32 30.9	PKS 2135−147	−24.7	−23.6	E	L	B97
21 43 38.3	+17 43 14.2	OX 169	−24.65	−23.26	E	L	TW
22 02 56.6	−56 59 10.7	MS 2159.5−5713	−20.80	−22.23	S	?	TW
22 03 15.0	+31 45 38.3	QSO 2201+315	−25.98	−24.69	E	L	TW
22 16 51.7	−18 48 14.0	Q 221652−184814	−23.15	−23.36	S	Q	TW
22 17 45.8	−03 32 47.1	Q 2215−037	−22.16	−23.47	E	Q	TW
22 50 27.5	+14 19 09.7	PKS 2247+14	−24.23	−23.65	E	L	TW
23 47 27.6	+18 44 06.9	Q 2344+184	−19.17	−22.70	S	Q	TW
23 51 53.0	−01 09 27.8	PKS 2349−014	−24.2	−24.5	IE	L	B97

¹Filter notes: objects were observed with *WFPC2* filters between F606W and F814W and transformed to obtain M_V .

²Morphologies: a) E=elliptical; b) S=spiral; c) EI=elliptical undergoing strong interaction; d) SI=spiral undergoing strong interaction; e) ES=elliptical with possible inner disk; f) IE=irregular that is best fit with an elliptical model; g) IS=irregular that is best fit with a spiral model.

³References: a) TW=this work; b) B97=Bahcall et al (1997); c) M99=McLure et al. (1999); d) HM95=Hutchings & Morris (1995); e) B98=Boyce et al. (1998); f) B96=Boyce et al. (1996); g) B99=Boyce, Disney, & Bleaken (1999).

Table 2. Kolmogorov-Smirnov Test Results for Subclass Comparison

Subclasses (number) ^a	D for $M_V(\text{host})$	p for $M_V(\text{host})$	D for $M_V(\text{nuc})$	p for $M_V(\text{nuc})$
LE (23), QE (23)	0.522	0.00215	0.348	0.09581
LE (23), QS (19)	0.702	0.00003	0.588	0.00074
QE (23), QS (19)	0.268	0.38604	0.284	0.31654
L (26), Q (42)	0.504	0.00031	0.423	0.00414
E (46), S (23)	0.478	0.00104	0.413	0.00714

^aLE=radio-loud QSOs in elliptical hosts; QE=radio-quiet QSOs in elliptical hosts; QS=radio-quiet QSOs in spiral hosts; L=radio-loud QSOs; Q=radio-quiet QSOs; E=elliptical hosts; S=spiral hosts.

Note. — The parameter D is the K-S statistic. The parameter p is the probability of obtaining D if the objects in both subclasses are drawn from the same parent population.